



# The effects of the crystallinity index of cellulose on the flexural properties of hybrid-cellulose epoxy composites

Nathawat POOPAKDEE<sup>1</sup>, and Warut THAMMAWICHAI<sup>1,\*</sup>

<sup>1</sup>Navaminda Kasatriyadhiraj Royal Air Force Academy, Mittraphap, Muak Lek District, Saraburi, 18180, Thailand

\*Corresponding author e-mail: warut\_t@rtaf.mi.th

**Received date:**

29 November 2023

**Revised date:**

16 March 2024

**Accepted date:**

24 May 2024

**Keywords:**

Crystallinity index;  
Hybrid-cellulose epoxy composite;  
Flexural properties;  
Interfacial bonding;  
Hydrogen bonding

**Abstract**

This work investigated the effects of the crystallinity index (CI) of cellulose on the flexural properties of hybrid-cellulose epoxy composites. The CI was varied by combining cellulose microfibrils (CMF) and microcrystalline cellulose (MCC), extracted from coir and eucalyptus, respectively, in various mixing ratios. From the XRD analysis, it was shown that the CI values and the CMF/MCC content follow a parabolic-fitting pattern, reaching a maximum value of 82.06% for the CMF/MCC of 30/70. The composites with cellulose of different CI values were fabricated and the flexural properties were measured. The results showed that the flexural strength increased as the CI increased, reaching a maximum of 105.45 MPa for a CI value of 81.87%. However, the flexural modulus displayed a parabolic relationship with respect to the CI value, reaching a maximum of 3,015.53 MPa for a CI value of 81.45%. FTIR spectroscopy was used to study the correlation between the interfacial bonding via hydrogen bonding of hydroxyl groups in cellulose and epoxy, the CI value, and the flexural properties. It was suggested that the strength of the cellulose was an important factor for the flexural strength of the composite, whereas both cellulose strength and interfacial bonding were crucial for the enhancement of the flexural modulus.

## 1. Introduction

Polymer composite materials have been extensively used in various industries [1]. This is due to their outstanding advantages over conventional materials, e.g., high strength-to-weight ratio, abrasion resistance, corrosion resistance, chemical resistance, smoother surfaces, and excellent design flexibility [2,3]. However, for demanding applications such as automobile and aerospace, the mechanical properties are usually the main factor to be considered. Though the mechanical properties of a composite are the combination of those of its constituents, reinforcement predominates over the matrix since it carries most of the load. Hence, an appropriate selection of material for use as a reinforcement is crucial.

Typically, there are two kinds of reinforcement: synthetic [4-8] and natural [9-11]. The commonly used synthetic reinforcement is glass, carbon, aramid, etc., whereas the natural ones are natural fibers and cellulose from plants or animals. Though synthetic ones have already been utilized extensively, natural fibers are also acquiring interest over the years [11-14]. Natural fibers, particularly cellulose fibers, have low density, better machinability, a more reactive surface, low price and good availability, decent mechanical properties, and better recycling capability [15-17]. More importantly, they are also abundant in nature, resulting in their low price. Cellulose can be derived from plants or animals. The plant-based cellulose can be extracted from, e.g., coir [9] and eucalyptus [18] which exists in two crystalline forms, i.e., cellulose I and cellulose II [19]. Figure 1 shows the chemical

structure of cellulose with the chemical formula  $[C_6H_{10}O_5]_n$ . They normally exist in the form of microfibril bundles enclosed by impurities, i.e., hemicellulose, lignin, pectin, wax, and other substances [4-8]. Various kinds of chemical treatments [9,18,20] are required to remove those impurities.

Cellulose is a polymer called polysaccharide made of thousands of repeating units of  $\beta$ -(1 $\rightarrow$ 4)-D-glucopyranose monomers [21]. The glycosidic linkage between pyranose rings forms a linear chain of a homopolymer with high rigidity [15]. The hydroxyl groups around the chain can form intermolecular hydrogen bonds between the chains, and intramolecular hydrogen bonds within the same chain as shown in Figure 2. The intermolecular hydrogen bonding between chains holds the cellulose molecules together closely resulting in highly ordered structures called crystalline regions as shown in Figure 3. This gives the microfibrils high strength. However, there are also regions with less ordered structures called amorphous regions, where the chains are less linked and further apart. Thus, there are more free hydroxyl groups available for bonding with other substances, e.g., with composite, the polymer matrix.

An interfacial bonding between the reinforcement and matrix is also equally important in determining the overall mechanical properties. A good interfacial bonding can help transfer load from the matrix to reinforcement more effectively. Generally, there are three main types of interfacial bonding: mechanical, physical, and chemical [22]. For a cellulose-reinforced polymer composite, the principal interfacial bonding is mechanical interlocking as well as physical bonding,

e.g., hydrogen bonding between fibers and matrix. The intermolecular hydrogen bonding between cellulose molecules and matrix depends on the number of interacting hydroxyl (-OH) groups. Although cellulose fibers have a high surface area and high tensile strength [23,24], their usability in a polymer matrix, e.g., polypropylene and epoxy, is still limited. This is because of their compatibility issues resulting in low dispersibility and low interfacial bonding, subsequently leading to poor mechanical properties. Various approaches were explored to solve this problem, but they involved the use of chemicals, e.g., compatibilizers, and surfactants [25-28]. This work will explore an alternative method to improve hydrogen bonding through manipulation of the crystallinity index (CI) of cellulose without involving chemicals and complicated procedures.

The CI of cellulose microfibrils is the ratio between the crystalline regions and amorphous regions. Cellulose microfibrils with more amorphous regions and fewer crystalline regions contain more free -OH groups to interact with the matrix, while the ones with fewer amorphous regions will contain fewer free -OH groups and will be less reactive [29,30]. Nevertheless, having too many amorphous regions will reduce the strength of the fibers, resulting in poorer mechanical properties [31]. Conversely, having too many crystalline regions will decrease the intermolecular hydrogen bonds with the matrix, which might result in poorer mechanical properties as well. Hence, by adjusting the CI of the cellulose reinforcement, we could optimize the mechanical properties of the composite, where a balance between interfacial bonding and reinforcement strength is achieved. One way to adjust the CI is to use ball milling [32, 33]. However, it is difficult to control the resultant CI. Owing to its highly destructive nature, fibers were damaged and broken very rapidly, resulting in a rapid reduction of CI value, thereby reducing the strength of the fibers dramatically.

In this work, we adjusted the CI of cellulose reinforcement by combining cellulose microfibrils (CMF) [9] extracted from coir and microcrystalline cellulose (MCC) [32,34,35] extracted from eucalyptus, which have different CI, in various mixing ratios. Then we investigated the effects of the CI on the mechanical properties of hybrid-cellulose epoxy composites. Moreover, the correlation between the hydrogen bonding of -OH groups in cellulose and epoxy molecules and the flexural properties of the composites was also explored.

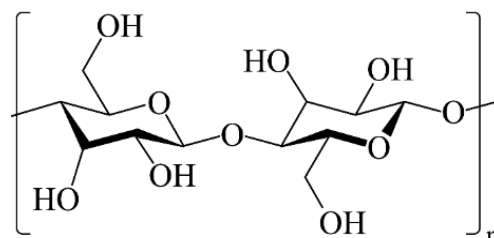


Figure 1. The chemical structure of a cellulose molecule.

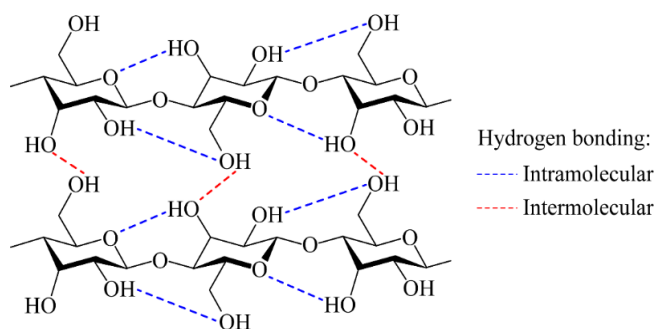


Figure 2. Intramolecular and intermolecular hydrogen bonding in cellulose molecules.

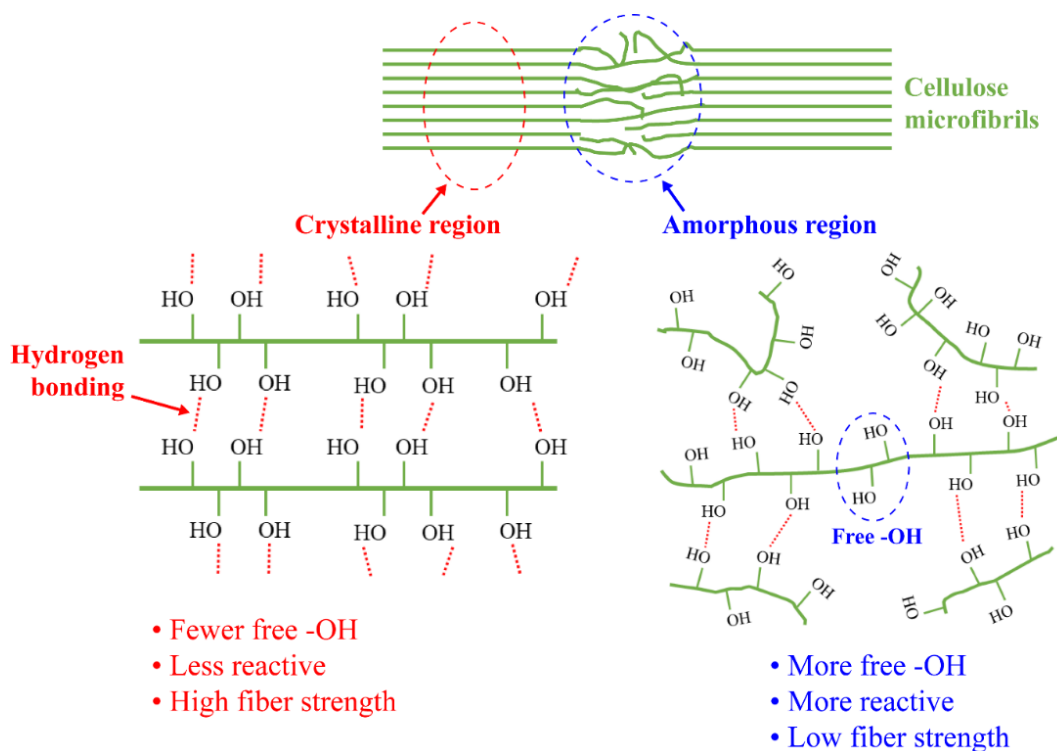


Figure 3. Crystalline and amorphous regions in cellulose microfibrils.

## 2. Experimental

### 2.1 Materials

The CMF was prepared in-house from a coconut coir purchased from a local source. The MCC was supplied by SCG Packaging Pub Co., Ltd. The epoxy resin was purchased from BRP Composite Part., Ltd.

### 2.2 Preparation of CMF

The CMF was prepared by first cutting the coir into shorter fibers, washing with boiled DI water, and drying in an oven at 70°C. With a coir-to-solution ratio of 1:70, the coir was then treated with 10% w/v NaOH at 90°C for 2 h. After that, the NaOH-treated fibers were thoroughly washed with DI water numerous times until pH 7 was achieved, and dried at 70°C. Next, with a fibers-to-solution ratio of 1:60, the NaOH-treated fibers were treated with 30 wt% H<sub>2</sub>O<sub>2</sub> at 90°C for 3.5 h. The H<sub>2</sub>O<sub>2</sub>-treated fibers were rinsed with DI water numerous times. After that, they were ultrasonicated in DI water at room temperature for 1 h using Elma Elmasonic E30H ultrasonic bath at 37 kHz. Finally, they were air-dried for 24 h.

### 2.3 Fabrication of hybrid-cellulose epoxy composites

CMF and MCC were combined in various mixing ratios, added into ethanol, and stirred at 500 rpm for 10 min using an IKA RW 20 digital overhead stirrer. The combined cellulose reinforcement was homogeneously dispersed in ethanol using a technique called "Couple Ultrasonication" [36]. This technique uses both ultrasonic bath (ELMA E 30 H Elmasonic) and ultrasonic probe systems at the same time. The ultrasonic probe system, Cole-Parmer 500 W Ultrasonic Homogenizer, comprises an ultrasonic processor model CP505 with an operating frequency of 20 kHz and a maximum power of 500 W, and an ultrasonic probe model CV334. The Couple Ultrasonication was performed with a probe amplitude of 60% and an ON/OFF pulse interval of 30/20 s for 30 min. After that, the ultrasonicated mixture was mixed with epoxide by stirring at 800 rpm for 5 min. The ethanol was then removed from the mixture by heating at 50°C using a hot plate while stirring at 500 rpm using an overhead stirrer. This process was performed until there was no more than 10 wt% of ethanol left in the mixture, which was determined by weighing. The mixture was then cooled down to room temperature. Later, the cellulose-epoxide mixture was couple-ultrasonicated for 30 min under the same conditions previously used and cooled down to room temperature before thoroughly mixing with hardener. The resin casting technique was used to fabricate the composite specimens for flexural properties testing according to ASTM D790 [37] with a span-to-thickness ratio

of 16:1, a span length of 48 mm, a thickness of 3 mm, an overall length of 90 mm, and a width of 12.7 mm. Table 1 shows the amounts of CMF, MCC and epoxy resin used for the fabrication of five composite test specimens. The total weight content of the combined cellulose reinforcement was kept at 2 wt%.

### 2.4 Characterizations

#### 2.4.1 Flexural properties testing

The flexural properties testing was performed using a universal testing machine (NRI-TS500-50B) according to procedure A specified in ASTM D790 [37]. The rate of crosshead motion of 1.28 mm·min<sup>-1</sup>, which results in a strain rate of 0.01 mm·min<sup>-1</sup>, was used. The force applied and the deflection depth of the specimens were recorded. The crosshead displacement was used as the deflection depth. The tests were carried out until the failure of the specimens was reached and repeated for five specimens. The stress-strain curves were plotted, and the flexural properties were analyzed.

#### 2.4.2 X-ray diffraction (XRD)

In this work, we examined the CI of the cellulose reinforcement by XRD employing a Rigaku SmartLab X-ray Diffractometer (Synchrotron Light Research Institute: SLRI). The test was performed in the range of x-ray diffraction angle (2θ) of 10° to 30° with a step width of 0.02° and a scan speed of 2.4225° per min. The XRD patterns were in the form of reflected intensities against 2θ angle. A peak height method [38, 39] was used for the determination of CI. The CI can be calculated by taking the difference between the intensity of the crystalline peak of the crystal plane (0 0 2), *I*<sub>002</sub>, at 2θ = 22.5° and that of the amorphous peak, *I*<sub>AM</sub>, at around 2θ = 18.0°–19.0°, and then divided by *I*<sub>002</sub> and times 100%, as shown in Equation (1).

$$CI = \frac{I_{002} - I_{AM}}{I_{002}} \times 100\% \quad (1)$$

#### 2.4.3 Fourier transform infrared spectroscopy (FTIR)

In this work, FTIR was used for two purposes. The first was to verify the product of the extracted cellulose and the removal of impurities, such as lignin and hemicellulose, from the cellulose microfibrils. The second was to investigate the hydrogen bonding between the cellulose reinforcement and epoxy matrix by tracking the characteristic peak at 3350 cm<sup>-1</sup> which corresponds to the vibration of –OH groups. The FTIR was performed in the range of 4000 cm<sup>-1</sup> to 800 cm<sup>-1</sup> using Bruker Tensor 27 spectrometer with Hyperion 3000-MCT microscope (SLRI) with a resolution of 4 cm<sup>-1</sup> and 64 scans. Diamond anvil cells and a Ge ATR-crystal were employed.

**Table 1.** Summary of the composition of cellulose-reinforced epoxy composite.

Mixing ratio (CMF/MCC)	Quantity (g)		
	CMF	MCC	Epoxy
100/0	0.61	0.00	29.89
75/25	0.46	0.16	29.89
50/50	0.31	0.31	29.89
30/70	0.19	0.43	29.89
0/100	0.00	0.61	29.89

### 2.4.4 Scanning electron microscopy (SEM)

The morphology of the untreated coir and extracted cellulose were examined using a Zeiss EVO 10 scanning electron microscope (Technical Division, Directorate of Armament, Royal Thai Air Force) operating at 25 kV.

## 3. Results and discussion

### 3.1 Characterizations of cellulose reinforcement

The CMF and MCC were examined by SEM analysis and FTIR spectroscopy to confirm that the impurities such as hemicellulose, lignin, wax were successfully removed, as shown in Figure 4 and Figure 5.

Figure 4 compares the photographs and SEM micrographs of the untreated coir fibers, the CMF, and the as-received MCC. Originally, the untreated fibers were light brown. They were bundles of cellulose microfibrils covered with hemicellulose, lignin, wax, etc., making their diameters as large as 100  $\mu\text{m}$ . After the chemical treatment, the fibers were an off-white color. The diameters were dramatically smaller, ranging from 14  $\mu\text{m}$  to 20  $\mu\text{m}$ . This suggests that the impurities were removed and individual microfibrils were separated. The as-received MCC was whiter and much shorter than the CMF. Figure 5 compares FTIR spectra of the untreated coir, the CMF, and the as-received MCC, in the wavenumber range 800  $\text{cm}^{-1}$  to 4000  $\text{cm}^{-1}$ . For the untreated coir, the spectrum shows a peak at 1738  $\text{cm}^{-1}$  which is attributed to the stretching vibrations of the C=O bonds of ketone, carbonyl, aliphatic, carboxylic and ester groups in hemicellulose, lignin, waxes, and fats [40–44]. Moreover, there are also peaks around 1649  $\text{cm}^{-1}$  to 1600  $\text{cm}^{-1}$  which correspond to aromatic ring vibration

in hemicellulose and lignin [42,45]. In addition, there is a peak at 1512  $\text{cm}^{-1}$  attributed to benzene ring stretching vibrations in lignin [45]. Another evidence of lignin and waxes present in the untreated coir is a peak around 1300  $\text{cm}^{-1}$  to 1200  $\text{cm}^{-1}$  which is attributed to the vibrations of the C–O bonds of the esters, ethers, and phenols [46] and aromatic skeletal vibration [47]. After the chemical treatment, those peaks are absent, indicating a removal of all impurities. The FTIR spectrum of MCC is similar to that of the CMF.

### 3.2 Crystallinity index of cellulose reinforcement

The cellulose reinforcements of CMF/MCC mixing ratios 100/0, 75/25, 50/50, 30/70, and 0/100 were examined by XRD. The XRD spectra are shown in Figure 6. The characteristic peaks of crystalline cellulose are shown at  $2\theta = 14.5^\circ$ ,  $16.5^\circ$ , and  $22.5^\circ$ , which correspond to the crystal planes (1 0 1), (1 0  $\bar{1}$ ) and (0 0 2), respectively [39]. Table 2 shows the crystallinity index of the cellulose reinforcements, which were calculated according to Equation (1).

The CI values were then plotted against the MCC content as a representation of CMF/MCC mixing ratios, as shown in Figure 7. The data points were also curve-fitted in a blue dashed line. The fitting results illustrating the relationship between the MCC content and CI values indicate that they follow a parabolic-fitting pattern. The 100/0 mixing ratio (100% CMF) exhibits the lowest CI of 75.21%. As the MCC content gets higher (lower CMF content), the CI reaches a maximum value of 82.06% at 30/70 mixing ratio, but then slightly declines to 81.81% at 0/100 mixing ratio. The reason for the higher CI value for the 30/70 mixing ratio might be that the small amount of CMF may interact with the MCC, and they interconnect to form a more rigid network via hydrogen bonding [48,49]. This demonstrates that CI was successfully adjusted by mixing CMF and MCC in various ratios.

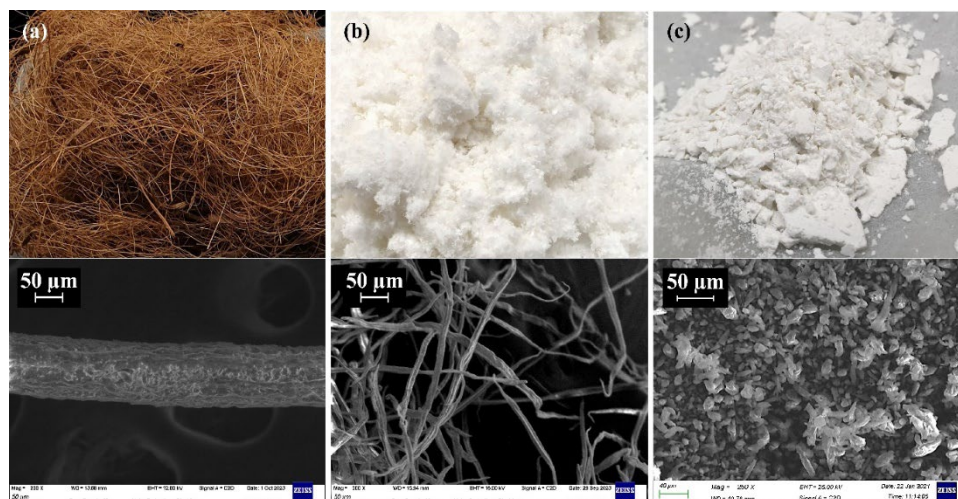


**Figure 4.** The photographs (top) and SEM micrographs (bottom) of the untreated coir (a), the CMF (b), and the as-received MCC (c).

**Table 2.** The crystallinity indexes of cellulose-reinforced epoxy composite at different CMF/MCC mixing ratios.

Mixing ratio (CMF/MCC)	Crystallinity index (%)
100/0	75.21
75/25	79.06
50/50	81.45
30/70	82.06
0/100	81.87

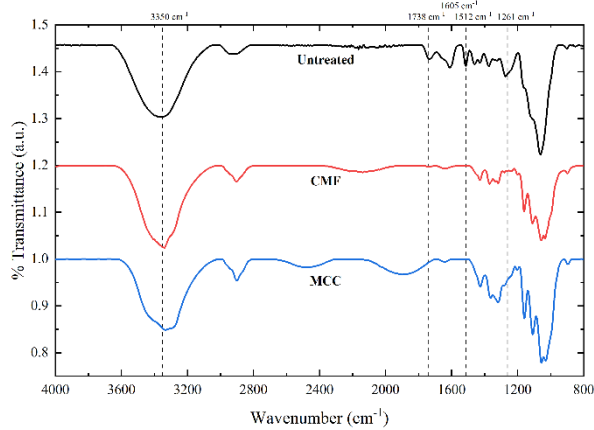


**Figure 5.** The FTIR spectra of the untreated coir (black solid line), the CMF (red solid line), and the as-received MCC (blue solid line).

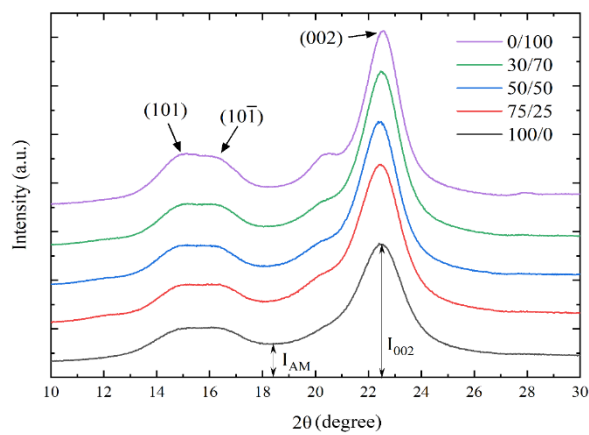


**Figure 6.** The XRD patterns of cellulose reinforcements with CMF/MCC mixing ratios 100/0 (black), 75/25 (red), 50/50 (blue), 30/70 (green), and 0/100 (purple).

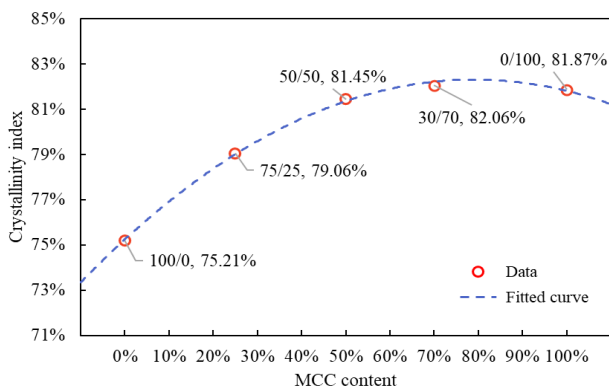


**Figure 7.** The crystallinity index of CMF/MCC cellulose reinforcement as a function of MCC content and the fitted curve (blue dashed line).

### 3.3 Mechanical properties

The flexural properties of the composite samples with the CMF/MCC mixing ratios 100/0, 75/25, 50/50, 30/70, and 0/100 were studied according to ASTM D790. Figure 8 shows the flexural stress-strain curves of the test results. The flexural properties were determined from the stress-strain curves and plotted as bar charts, as shown in

Figure 9-11. The flexural stress-strain curves show a rather obvious trend regarding the change in the CMF/MCC mixing ratio. The flexural strength increases as MCC increases and CMF decreases. The results as shown in Figure 8 and Figure 9 demonstrate that the addition of MCC improves the flexural strength of epoxy composites. The highest value is reached by the composition with a 0/100 mixing ratio.

For the flexural strain, the 0/100 sample shows the broadest plastic deformation region. This region then vanishes when the CMF content is higher than 30%. As shown in Figure 10, the 0/100 sample shows the highest flexural strain-at-maximum of 6.5% and strain-at-break of 9.5%. The 100/0 sample shows the lowest flexural strain of 3%. This suggests that an increase in CMF content can reduce the plastic deformation region.

The slope of the flexural stress-strain curve signifies the flexural modulus of a material. The slope of the curves gets steeper when increasing MCC content from 100/0 towards 50/50 where the slope is steepest. Hence, Figure 11 shows that the modulus increases to 50/50 mixing ratio and then decreases as the amount of MCC increases. The 50/50 has the highest flexural modulus of about 3,000 MPa. The steepness of the slope then declines for the 30/70 sample and the lowest for the 100/0 sample. Thus, the flexural modulus of the composite does not simply follow the amount of CMF or MCC. This might be also attributed to the interfacial bonding between reinforcement and matrix, as will be discussed later.

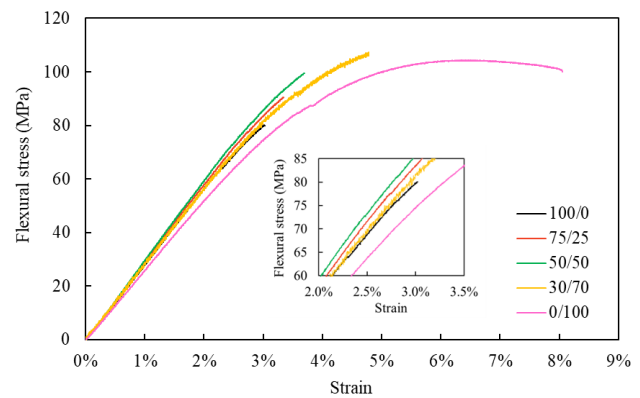


**Figure 8.** Flexural stress-strain curves of the composite samples with the CMF/MCC mixing ratios of 100/0 (black), 75/25 (red), 50/50 (green), 30/70 (yellow) and 0/100 (pink).

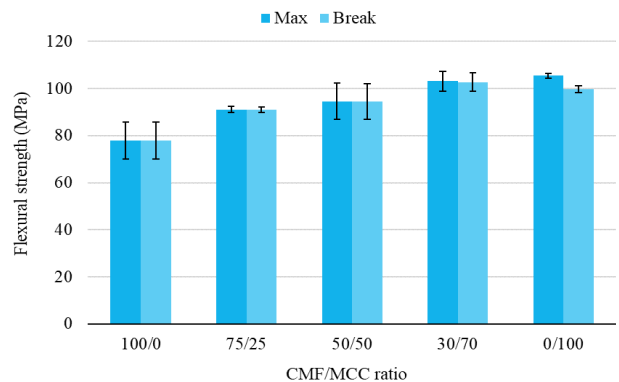


**Figure 9.** Flexural stress-at-maximum and stress-at-break of the composite samples with the CMF/MCC mixing ratios of 100/0, 75/25, 50/50, 30/70, and 0/100.

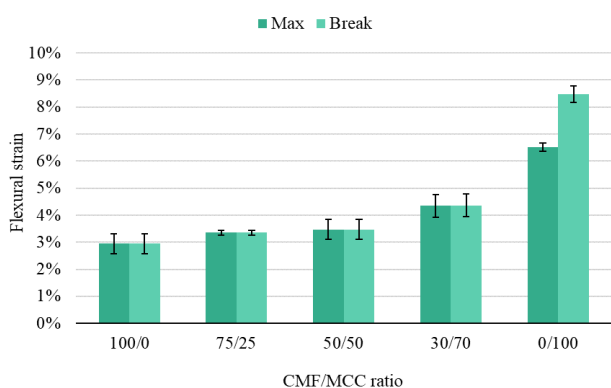


**Figure 10.** Flexural strain-at-maximum and strain-at-break of the composite samples with the CMF/MCC mixing ratios of 100/0, 75/25, 50/50, 30/70 and 0/100.

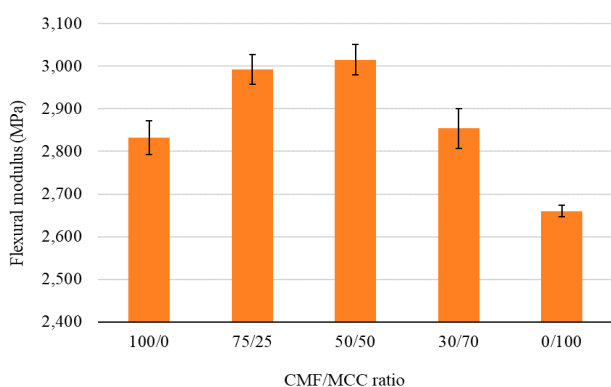


**Figure 11.** Flexural modulus of the composite samples with the CMF/MCC mixing ratios of 100/0, 75/25, 50/50, 30/70, and 0/100.

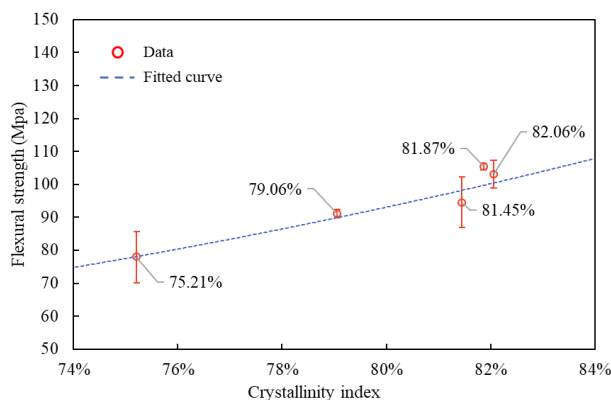


**Figure 12.** Flexural strength of the composites versus CI of the cellulose reinforcement and the fitted curve (blue dashed line).

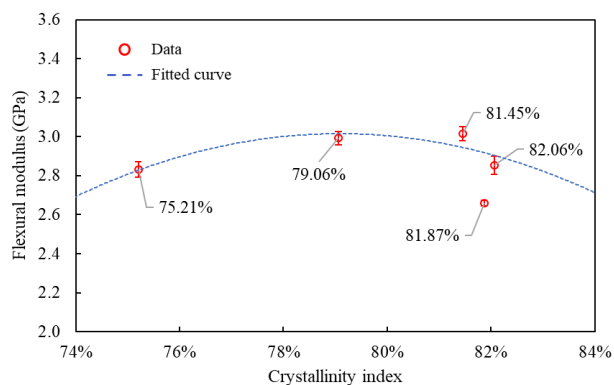


**Figure 13.** Flexural modulus of the composites versus CI of the cellulose reinforcement and the fitted curve (blue dashed line).

### 3.4 Effect of crystallinity index on mechanical properties

In this section, we investigate the correlation between the CI and the mechanical properties of the corresponding composites. The CI, flexural strength and flexural modulus of the corresponding composites reinforced with different CMF/MCC mixing ratios are shown in Table 3.

The flexural properties were plotted against the CI, as shown in Figure 12 and Figure 13. The fitting results of the relationship between the flexural strength and CI exhibit proportionality; the flexural strength increases as the CI increases. However, the relationship between flexural modulus and CI follows a parabolic-fitting pattern. The flexural modulus gradually increases as CI increases from 75.21% and reaches its peak when CI is approximately 79%. It is then lower when the CI is higher.

### 3.5 Interfacial interaction via hydrogen bonding

We investigated the interfacial bonding via hydrogen bonds between the cellulose and epoxy with FTIR spectroscopy. The hydrogen bonding is observable through the absorption band for the hydroxyl ( $-OH$ ) group in the FTIR spectrum. The spectra of the neat sample (EP) and the hybrid-cellulose epoxy composite samples were compared in Figure 14. The composite samples are 100/0-EP, 75/25-EP, 50/50-EP, 30/70-EP, and 0/100-EP. The  $-OH$  characteristic peaks in the FTIR spectra for each sample were plotted in the range of  $3600\text{ cm}^{-1}$  to  $3050\text{ cm}^{-1}$  with an inset showing the full range of spectrum of  $4000\text{ cm}^{-1}$  to  $700\text{ cm}^{-1}$ . Typically, free  $-OH$  groups exhibit a narrow and strong characteristic absorption peak because of the stretching vibrations of the  $O-H$  bond around  $3600\text{ cm}^{-1}$  [50]. However,

**Table 3.** The crystalline index and flexural properties of epoxy composite reinforced with different CMF/MCC mixing ratios

CMF/MCC	CI (%)	Strength (MPa)	Modulus (MPa)
100/0	75.21	$77.89 \pm 7.80$	$2,832.38 \pm 39.87$
75/25	79.06	$91.13 \pm 1.24$	$2,992.63 \pm 35.22$
50/50	81.45	$94.51 \pm 7.69$	$3,015.53 \pm 35.44$
30/70	82.06	$103.11 \pm 4.27$	$2,853.93 \pm 46.21$
0/100	81.87	$105.45 \pm 1.01$	$2,660.14 \pm 13.59$

the formation of hydrogen bonds will lead to a shift slightly to a lower wavenumber, a broadening of the peak, and a change in the peak intensity of the absorption band [40,42,47,51-53]. This is because cooperative hydrogen bonding increases the O–H bond length while causing the weakening of the O–H bond [54]. Consequently, the stretching vibration frequency is lower. In the present work, the –OH stretching peak is observed around  $3350\text{ cm}^{-1}$  [51].

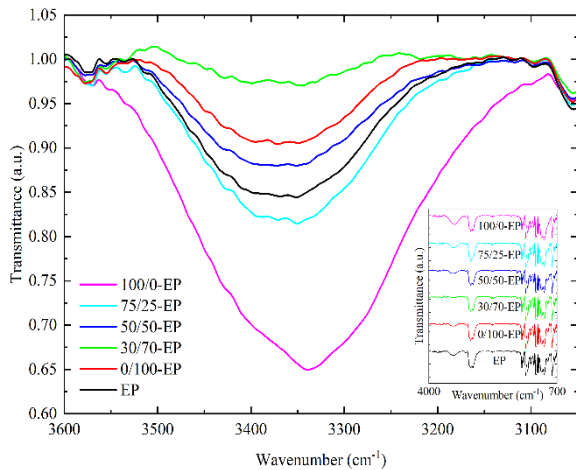


**Figure 14.** The FTIR spectra of the neat epoxy (EP, black) and the hybrid-cellulose epoxy composites 100/0-EP (pink), 75/25-EP (cyan), 50/50-EP (blue), 30/70-EP (green), and 0/100-EP (red).

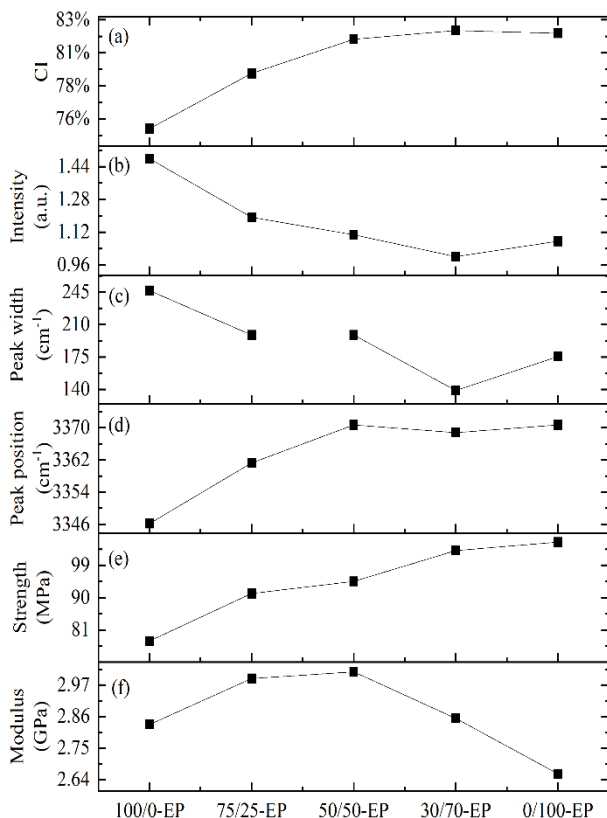


**Figure 15.** The CI of cellulose (a), normalized intensity (b), full-width half maximum (c), position (d) of the –OH characteristic peaks in the FTIR spectra, and the flexural strength (e) and flexural modulus (f) of the hybrid-cellulose epoxy composites.

By observing the change in peak intensity, peak width, and peak position, the hydrogen bonding of the –OH groups can be analyzed. In order to study the correlation between the CI and hydrogen bonding and their effects on the flexural properties of the hybrid-cellulose epoxy composite, peak height, peak position, and full-width half maximum (FWHM) were decomposed using Gaussian deconvolution. Figure 15 shows the comparison of the degree of crystallinity, the normalized peak height, peak position, and full-width half maximum of the Gaussian-fitted peaks of the O–H stretching mode of the hybrid-cellulose composites compared with flexural strength and flexural modulus. As shown in Figure 15, the peak intensity is weakened, and the peak width becomes narrower as the CI value is higher, whereas the peak position is shifted toward a higher frequency. The 100/0-EP has the strongest and broadest –OH peak and the largest shift to the lower wavenumber. This indicates that there are a lot of free –OH groups from the CMF forming either intramolecular or intermolecular hydrogen bonding. This agrees well with the lowest CI value of the CMF. With the increasing CI value from 79.06% for the 75/25-EP to 81.45% for 50/50-EP, there was a weakening of peak intensities, narrowing down of the band, and peak shifting to higher wavenumber. This suggests a decrease in the number of –OH groups forming hydrogen bonding and weakening of hydrogen bonding [32,54-56]. When the CI value increases from 81.45% for the 50/50-EP to 82.06% for the 30/70-EP and to 81.87% for the 0/100-EP, there is a slight decrease in peak intensity and a smaller shift in peak position. However, the peak width of the 30/70-EP is significantly smaller than those of 50/50-EP and 0/100-EP.

The CMF has a high surface area with an enormous amount of hydroxyl groups [54], which reacts with epoxides with less amount of hydroxyl groups [57]. Hence, this leads to the strong tendency to form intermolecular hydrogen bonding with each other, which could contribute to the steric hindrance [58] lowering interfacial bonding, together with lower fiber strength due to low CI, thereby contributing to the lowest flexural strength [41,56]. As the CI gets higher from 79.06% for the 75/25-EP to 82.06% for 30/70-EP, the number of free –OH is lower while the strength of the cellulose is higher. As a result, the flexural strength is higher. The 0/100-EP sample has the highest flexural strength because the MCC has high CI (fewer free –OH and high fiber strength). This suggests that the flexural strength of the hybrid-cellulose epoxy composite largely depends on the strength of the cellulose, rather than the interfacial bonding.

The flexural modulus is lower for the 100/0-EP due to a similar reason as with flexural strength. There are enormous amount of –OH groups in the CMF [54] forming hydrogen bonding with each other rather than with epoxy [57,58], thereby lowering interfacial bonding, resulting in a decrease in the flexural modulus of the composite. The flexural modulus is higher for the 75/25-EP and reaches the maximum for the 50/50-EP. This is because of the lowering of CMF content in the composite, which results in a reducing amount of free –OH groups, and the raising of MCC content, which results in an increase in the strength of reinforcement. In addition, the formation of the rigid network of cellulose reinforcement via hydrogen bonding is one of the keys to the enhancement of the elastic modulus of the composite [48,49]. The 50/50-EP sample may have a suitable amount of free –OH groups from CMF and MCC that can interact with each other, forming a stronger network, while also forming hydrogen bonds

with epoxy. The flexural modulus of 30/70-EP and 0/100-EP drops dramatically, albeit with a relatively higher fiber strength (higher CI). This may be because of the low aspect ratio of the MCC and a reducing amount of free –OH groups that prevent them from forming a solid network between themselves and with the epoxy, which will subsequently diminish the mechanical properties [59]. In conclusion, the CI value of 81.45% (50/50-EP) appears to be the sweet spot for enhancing the flexural modulus where the balance between the strength of reinforcement and hydrogen bonding is achieved.

#### 4. Conclusions

This work studied the effects of the crystallinity index of cellulose reinforcement on the flexural properties of the hybrid-cellulose epoxy composites. The CI of the cellulose reinforcement was varied by combining two types of cellulose: cellulose microfibrils from coir and microcrystalline cellulose from eucalyptus in various mixing ratios. The flexural properties of the cellulose composites were measured and the correlations between the CI, the flexural properties, and the interfacial bonding via hydrogen bonding were examined using FTIR spectroscopy. The results showed that the cellulose reinforcement with a higher degree of CI (higher fiber strength) enhanced the flexural strength of the composite, i.e., the flexural strength increased as the CI values increased proportionally. In contrast, both fiber strength and interfacial bonding played a critical role in the enhancement of the flexural modulus. The flexural modulus displayed a parabolic relationship with respect to the CI value. The flexural modulus was highest when the CI value reached 81.45% (50/50-EP) and it was lower when the CI value was higher or lower. It appears that at this CI value, the balance between the strength of reinforcement and hydrogen bonding is achieved.

#### Acknowledgements

We would like to express our gratitude towards SCG Packaging PCL for the supplement of microcrystalline cellulose. We are grateful to Duangjai Srisamut and the Synchrotron Light Research Institute (Public Organization), Nakhon Ratchasima, Thailand, for the XRD and FTIR characterizations. We are thankful to Flt Lt Suthatsana Homthian and the Technical Division, Directorate of Armament, Royal Thai Air Force, for technical support with SEM characterization. Also, we would like to show our appreciation to Assoc. Prof. Gp Capt Somkiat Sukanghong, Assoc. Prof. Gp Capt Kitti Srinuchasart, Assist. Prof. Gp Capt Sansanee Haemakom, and for their helpful support. This work is funded by the Royal Thai Air Force.

#### References

- [1] S. S. Godara, A. Yadav, B. Goswami, and R. S. Rana, "Review on history and characterization of polymer composite materials," *Materials Today: Proceedings*, vol. 44, pp. 2674-2677, 2021.
- [2] C. Wu, F. Xu, H. Wang, H. Liu, F. Yan, and C. Ma, "Manufacturing technologies of polymer composites-A review," *Polymers (Basel)*, vol. 15, no. 3, p. 712, 2023.
- [3] K. K. Chawla, "Introduction," in *Composite Materials: Science and Engineering*, K. K. Chawla Ed. Cham: Springer International Publishing, 2019, pp. 3-6.
- [4] M. Z. Rong, M. Q. Zhang, Y. Liu, G. C. Yang, and H. M. Zeng, "The effect of fiber treatment on the mechanical properties of unidirectional sisal-reinforced epoxy composites," *Composites Science and Technology*, vol. 61, no. 10, pp. 1437-1447, 2001.
- [5] M. R. Vignon, L. Heux, M. E. Malainine, and M. Mahrouz, "Arabian-cellulose composite in *Opuntia ficus-indica* prickly pear spines," *Carbohydrate Research*, vol. 339, no. 1, pp. 123-131, 2004.
- [6] A. K. Bledzki, S. Reihmane, and J. Gassan, "Properties and modification methods for vegetable fibers for natural fiber composites," *Journal of Applied Polymer Science*, vol. 59, no. 8, pp. 1329-1336, 1996.
- [7] K. G. Satyanarayana, K. Sukumaran, P. S. Mukherjee, C. Pavithran, and S. G. K. Pillai, "Natural fibre-polymer composites," *Cement and Concrete Composites*, vol. 12, no. 2, pp. 117-136, 1990.
- [8] A. Bismarck, S. Mishra, and T. Lampke, "Plant fibers as reinforcement for green composites," in *Natural Fibers, Biopolymers, and Biocomposites*, A. K. Mohanty, M. Misra, and L. T. Drzal Eds. Boca Raton: CRC Press, 2005, pp. 37-108.
- [9] W. Thammawichai, N. Poopakdee, C. Suwanchawalit, and K. Suwatpipat, "Synthesis and characterization of cellulose-microfibril reinforced epoxy composite," in *2015 Asian Conference on Defence Technology (ACDT)*, pp. 180-182.
- [10] M. M. Thwe and K. Liao, "Durability of bamboo-glass fiber reinforced polymer matrix hybrid composites," *Composites Science and Technology*, vol. 63, no. 3, pp. 375-387, 2003.
- [11] A. R. Bhat, R. Kumar, and P. K. S. Mural, "Natural fiber reinforced polymer composites: A comprehensive review of Tribo-Mechanical properties," *Tribology International*, vol. 189, p. 108978, 2023.
- [12] R. A. Kurien, M. Maria Anil, S. L. Sharan Mohan, and J. Anna Thomas, "Natural fiber composites as sustainable resources for emerging applications- a review," *Materials Today: Proceedings*, 2023.
- [13] L. Chen, Z. Chen, Z. Xie, L. Wei, J. Hua, L. Huang, and P.-S. Yap, "Recent developments on natural fiber concrete: A review of properties, sustainability, applications, barriers, and opportunities," *Developments in the Built Environment*, p. 100255, 2023.
- [14] I. Elfaleh, F. Abbassi, M. Habibi, F. Ahmad, M. Guedri, M. Nasri, and C. Garnier, "A comprehensive review of natural fibers and their composites: An eco-friendly alternative to conventional materials," *Results in Engineering*, vol. 19, p. 101271, 2023.
- [15] P. M. Visakh and S. Thomas, "Preparation of bionanomaterials and their polymer nanocomposites from waste and biomass," *Waste and Biomass Valorization*, vol. 1, no. 1, pp. 121-134, 2010.
- [16] J. R. Collier, M. Lu, M. Fahrurrozi, and B. J. Collier, "Cellulosic reinforcement in reactive composite systems," *Journal of Applied Polymer Science*, vol. 61, no. 8, pp. 1423-1430, 1996.

- [17] I. Aranberri-Askargorta, T. Lampke, and A. Bismarck, "Wetting behavior of flax fibers as reinforcement for polypropylene," *Journal of Colloid and Interface Science*, vol. 263, no. 2, pp. 580-589, 2003.
- [18] N. Rehman, Alam, N. Amin, I. Mian, and H. Ullah, "Ecofriendly isolation of cellulose from eucalyptus lenceolata : A novel approach," *International Journal of Polymer Science*, vol. 2018, pp. 1-7, 2018.
- [19] S. Kuga and R. Malcolm Brown, "Silver labeling of the reducing ends of bacterial cellulose," *Carbohydrate Research*, vol. 180, no. 2, pp. 345-350, 1988.
- [20] N. Abzan, A. Abbasian, M. Jonoobi, and I. Ghasemi, "Cellulose microfibril extraction from leftover celery pulp: Chemomechanical treatments, structural, morphological, and thermal characterization," *International Journal of Biological Macromolecules*, vol. 253, p. 126834, 2023.
- [21] R. L. Crawford, *Lignin biodegradation and transformation*. New York: John Wiley & Sons Inc, 1981, p. 170.
- [22] K. K. Chawla, "Interfaces," in *Composite Materials: Science and Engineering*, K. K. Chawla Ed. Cham: Springer International Publishing, 2019, pp. 107-136.
- [23] K. Tashiro and M. Kobayashi, "Lattice-dynamical prediction of the limiting Young's modulus of liquid crystalline arylate polymers: comparison with typical rigid-rod polymers," *Polymer*, vol. 32, no. 3, pp. 454-463, 1991.
- [24] M. Grunert and W. T. Winter, "Nanocomposites of cellulose acetate butyrate reinforced with cellulose nanocrystals," *Journal of Polymers and the Environment*, vol. 10, no. 1, pp. 27-30, 2002.
- [25] M. A. S. Azizi Samir, F. Alloin, and A. Dufresne, "Review of recent research into cellulosic whiskers, their properties and their application in nanocomposite field," *Biomacromolecules*, vol. 6, no. 2, pp. 612-626, 2005.
- [26] A. K. Bledzki and J. Gassan, "Composites reinforced with cellulose based fibres," *Progress in Polymer Science*, vol. 24, no. 2, pp. 221-274, 1999.
- [27] P. V. Joseph, K. Joseph, and S. Thomas, "Short sisal fiber reinforced polypropylene composites: The role of interface modification on ultimate properties," *Composite Interfaces*, vol. 9, no. 2, pp. 171-205, 2002.
- [28] A. Amash, and P. Zugenmaier, "Morphology and properties of isotropic and oriented samples of cellulose fibre-polypropylene composites," *Polymer*, vol. 41, no. 4, pp. 1589-1596, 2000.
- [29] S. Dumitriu and E. Chornet, "Polysaccharides as support for enzyme and cell immobilization," *Polysaccharides*, pp. 629-748, 1998.
- [30] W. Qiu, T. Endo, and T. Hirotsu, "Interfacial interactions of a novel mechanochemical composite of cellulose with maleated polypropylene," *Journal of Applied Polymer Science*, vol. 94, no. 3, pp. 1326-1335, 2004.
- [31] Z. Ling, T. Wang, M. Makarem, M. Santiago Cintrón, H. N. Cheng, X. Kang, M. Bacher, A. Potthast, T. Rosenau, H. King, C. D. Delhom, S. Nam, J. Vincent Edwards, S. H. Kim, F. Xu, and A. D. French, "Effects of ball milling on the structure of cotton cellulose," *Cellulose*, vol. 26, no. 1, pp. 305-328, 2019.
- [32] T. Huang, I. Kwan, K. D. Li, and M. Ek, "Effect of cellulose oxalate as cellulosic reinforcement in ternary composites of polypropylene/maleated polypropylene/cellulose," *Composites Part A: Applied Science and Manufacturing*, vol. 134, p. 105894, 2020.
- [33] M. L. Nelson and R. T. O'Connor, "Relation of certain infrared bands to cellulose crystallinity and crystal lattice type. Part II. A new infrared ratio for estimation of crystallinity in celluloses I and II," *Journal of Applied Polymer Science*, vol. 8, no. 3, pp. 1325-1341, 1964.
- [34] Q. Wu, M. Henriksson, X. Liu, and L. A. Berglund, "A high strength nanocomposite based on microcrystalline cellulose and polyurethane," *Biomacromolecules*, vol. 8, no. 12, pp. 3687-3692, 2007.
- [35] A. Ashori, and A. Nourbakhsh, "Performance properties of microcrystalline cellulose as a reinforcing agent in wood plastic composites," *Composites Part B: Engineering*, vol. 41, no. 7, pp. 578-581, 2010.
- [36] N. Poopakdee and W. Thammawichai, "Fabrication and mechanical properties of multi-walled carbon nanotube and cellulose microfibril reinforced epoxy composite," *International Journal of Mechanical and Production Engineering (IJMPE)*, vol. 7, no. 12, pp. 39-43, 2019.
- [37] *Standard Test Methods for Flexural Properties of Unreinforced and Reinforced Plastics and Electrical Insulating Materials*, ASTM D790, 2017.
- [38] L. Y. Mwaikambo, and M. P. Ansell, "Chemical modification of hemp, sisal, jute, and kapok fibers by alkalization," *Journal of Applied Polymer Science*, vol. 84, no. 12, pp. 2222-2234, 2002.
- [39] S. Park, J. O. Baker, M. E. Himmel, P. A. Parilla, and D. K. Johnson, "Cellulose crystallinity index: Measurement techniques and their impact on interpreting cellulase performance," *Biotechnology for Biofuels*, vol. 3, no. 1, p. 10, 2010.
- [40] H. Yang, R. Yan, H. Chen, D. H. Lee, and C. Zheng, "Characteristics of hemicellulose, cellulose and lignin pyrolysis," *Fuel*, vol. 86, no. 12, pp. 1781-1788, 2007.
- [41] V. A. Alvarez, and A. Vázquez, "Influence of fiber chemical modification procedure on the mechanical properties and water absorption of MaterBi-Y/sisal fiber composites," *Composites Part A: Applied Science and Manufacturing*, vol. 37, no. 10, pp. 1672-1680, 2006.
- [42] R. Javier-Astete, J. Jimenez-Davalos, and G. Zolla, "Determination of hemicellulose, cellulose, holocellulose and lignin content using FTIR in Calycophyllum spruceanum (Benth.) K. Schum. and Guazuma crinita Lam," *PLOS ONE*, vol. 16, no. 10, p. e0256559, 2021.
- [43] A. M. Raspolli Galletti, A. D'Alessio, D. Licursi, C. Antonetti, G. Valentini, A. Galia, and N. Nasso, "Midinfrared FT-IR as a tool for monitoring herbaceous biomass composition and its conversion to furfural," *Journal of Spectroscopy*, vol. 2015, p. 719042, 2015.
- [44] L. Chen, J. Y. Zhu, C. Baez, P. Kitin, and T. Elder, "Highly thermal-stable and functional cellulose nanocrystals and nanofibrils produced using fully recyclable organic acids," *Green Chemistry*, vol. 18, no. 13, pp. 3835-3843, 2016.

- [45] Adapa, L. Tabil, G. J. Schoenau, T. Canam, and T. Dumonceaux, "Quantitative analysis of lignocellulosic components of non-treated and steam exploded Barley, Canola, Oat and wheat straw using Fourier Transform Infrared Spectroscopy," *Journal of Agricultural Science and Technology*, vol. B1, pp. 177-188, 2011.
- [46] P. J. Herrera-Franco and A. Valadez-González, "A study of the mechanical properties of short natural-fiber reinforced composites," *Composites Part B: Engineering*, vol. 36, no. 8, pp. 597-608, 2005.
- [47] E. Abraham, B. Deepa, L. A. Pothan, M. Jacob, S. Thomas, U. Cvelbar, and R. Anandjiwala, "Extraction of nanocellulose fibrils from lignocellulosic fibres: A novel approach," *Carbohydrate Polymers*, vol. 86, no. 4, pp. 1468-1475, 2011.
- [48] A. Šturová, G. R. Davies, and S. J. Eichhorn, "Elastic modulus and stress-transfer properties of tunicate cellulose whiskers," *Biomacromolecules*, vol. 6, no. 2, pp. 1055-1061, 2005.
- [49] Y. Habibi, L. A. Lucia, and O. J. Rojas, "Cellulose nanocrystals: Chemistry, self-assembly, and applications," *Chemical Reviews*, vol. 110, no. 6, pp. 3479-3500, 2010.
- [50] S. Cichosz and A. Masek, "IR study on cellulose with the varied moisture contents: Insight into the supramolecular structure," *Materials*, vol. 13, no. 20, 2020.
- [51] S. Y. Oh, D. I. Yoo, Y. Shin, and G. Seo, "FTIR analysis of cellulose treated with sodium hydroxide and carbon dioxide," *Carbohydrate Research*, vol. 340, no. 3, pp. 417-428, 2005.
- [52] E. Abraham, B. Deepa, L. A. Pothan, J. Cintil, S. Thomas, M. J. John, R. Anandjiwala, and S. S. Narine, "Environmental friendly method for the extraction of coir fibre and isolation of nanofibre," *Carbohydrate Polymers*, vol. 92, no. 2, pp. 1477-1483, 2013.
- [53] M. G. Pineda-Pimentel, N. Flores-Ramirez, J. C. Farias Sanchez, L. Domratcheva-Lvova, S. R. Vasquez-Garcia, and L. Garcia-Gonzalez, "Theoretical analysis and FTIR of cellulose nanowhiskers/Poly(ButylAcrylate)," *Superficies y Vacío*, vol. 29, no. 3, pp. 83-86, 2016.
- [54] Y. Nishiyama, "Structure and properties of the cellulose microfibril," *Journal of Wood Science*, vol. 55, no. 4, pp. 241-249, 2009.
- [55] Y. Zheng, Z. Fu, D. Li, and M. Wu, "Effects of ball milling processes on the microstructure and rheological properties of microcrystalline cellulose as a sustainable polymer additive," *Materials*, vol. 11, no. 7, 2018.
- [56] Z. Liao, Z. Huang, H. Hu, Y. Zhang, and Y. Tan, "Microscopic structure and properties changes of cassava stillage residue pretreated by mechanical activation," *Bioresource Technology*, vol. 102, no. 17, pp. 7953-7958, 2011.
- [57] S. Dmitro, S. Sergej, B. Valerii, Y. Olha, R. Maria, S. Alexandra, and L. Y. Kokhtych, "Resistance and strength of bio-compatible epoxy- cellulose composites, as a function of concentration and dispersity of cellulose filler," *Biomedical Journal of Scientific & Technical Research*, vol. 31, no. 3, pp. 24211-24218, 2020.
- [58] S. Nakamura, Y. Tsuji, and K. Yoshizawa, "Role of hydrogen-bonding and OH- $\pi$  interactions in the adhesion of epoxy resin on hydrophilic surfaces," *ACS Omega*, vol. 5, no. 40, pp. 26211-26219, 2020.
- [59] W. Qiu, F. Zhang, T. Endo, and T. Hirotsu, "Milling-induced esterification between cellulose and maleated polypropylene," *Journal of Applied Polymer Science*, vol. 91, no. 3, pp. 1703-1709, 2004.